Negative Virial Coefficients and the Dominance of Loose Packed Diagrams for *D*-Dimensional Hard Spheres

N. Clisby[1] **and B. M. McCoy**[1]

We study the virial coefficients B_k of hard spheres in D dimensions by means of Monte-Carlo integration. We find that B_5 is positive in all dimensions but that B_6 is negative for all $D \geqslant 6$. For $7 \leqslant k \leqslant 17$ we compute sets of Ree–Hoover diagrams and find that either for large D or large k the dominant diagrams are "loose packed." We use these results to study the radius of convergence and the validity of the many approximations used for the equations of state for hard spheres.

1. INTRODUCTION

The question of the possible negativity of virial coefficients B_k in the low density expansion

$$\frac{P}{k_B T} = \rho + \sum_{k=2}^{\infty} B_k \rho^k \tag{1}$$

of the system of hard spheres with diameter σ in D dimensions specified by the two body pair potential

$$U(\mathbf{r}) = \begin{cases} +\infty & |\mathbf{r}| < \sigma \\ 0 & |\mathbf{r}| > \sigma \end{cases} \tag{2}$$

---

[1] C. N. Yang Institute for Theoretical Physics, State University of New York at Stony Brook, Stony Brook, New York 11794-3840; e-mail: Nathan.Clisby@stonybrook.edu and mccoy@insti.physics.sunysb.edu

Table I.   Numerical Values of the Virial Coefficients
B_k/B_2^{k-1} for $k=3,\ldots,8$ for $D=2, 3, 4, 5$

	discs	spheres
B_2	$\pi\sigma^2/2$	$2\pi\sigma^3/3$
B_3/B_2^2	$0.782004\cdots$ [3]	0.625 [4]
B_4/B_2^3	$0.5322318\cdots$ [5, 6]	$0.2869495\cdots$ [4, 7, 8]
B_5/B_2^4	$0.33355604(4)$ [9, 10]	$0.110252(1)$ [9, 11]
B_6/B_2^5	$0.19883(1)$ [9, 12]	$0.038808(55)$ [9, 13]
B_7/B_2^6	$0.114877(11)$ [13–15]	$0.013046(22)$ [13–15]
B_8/B_2^7	$0.065030(31)$ [13, 15]	$0.004164(16)$ [13, 15]
	$D=4$	$D=5$
B_2	$\pi^2\sigma^4/4$	$4\pi^2\sigma^5/15$
B_3/B_2^2	$0.50634\cdots$ [16]	$0.414062\cdots$ [16]
B_4/B_2^3	$0.15184606\cdots$ [17]	$0.075972512(4)$ [18]
B_5/B_2^4	$0.03563(7)$ [18]	$0.01287(6)$ [18]
B_6/B_2^5	$0.007691(28)$ [18]	$0.000942(27)$ [18]

has been an unresolved problem of outstanding importance since it was first proposed by Temperley[1] in 1957. For dimensions $D \leqslant 5$ all currently available information is summarized in Table I where it is seen that all B_k are positive. However it was first shown[2] in 1964 for $D \geqslant 8$ that B_4 is indeed negative. The best available current results for B_4 as a function of dimension are shown in Table II.

Most of our intuition and physical insight into the low density (fluid) phase of hard spheres in 3 dimensions comes from the 8 term virial expansion of Table I. Over the years this data has been used to produce many approximate equations of state.[9, 13, 19–33] These approximates all incorporate the feature of positive virial coefficients and they all have the feature that they have a radius of convergence which is greater than the packing fraction $\eta_{\mathrm{f}} = 0.49$ at which freezing has been seen to occur in computer experiments[24, 34, 35] where the packing fraction η is related to the density ρ by $\eta = B_2\rho/2^{D-1}$. This analyticity at the freezing density is incorporated into most phenomenological theories of freezing[36–38] as a homogeneity or mean field approximation which ignores the fluctuations at phase coexistence between the fluid and solid phases.[39]

However, if there are negative virial coefficients for hard spheres in $D=3$ then no conclusion on the radius of convergence of the virial expansion based on Table I can be considered as reliable.

The most striking effect of negative viral coefficients will occur if the signs oscillate with some period as $k \to \infty$ because this will give a radius of

Table II. Exact and Numerical Results for B_2, B_3, and B_4 for $2 \leqslant D \leqslant 12$

D	B_2	B_3/B_2^2	B_4/B_2^3 exact and numerical	
2	$\dfrac{\pi\sigma^2}{2}$	$\dfrac{4}{3} - \dfrac{\sqrt{3}}{\pi}$	$2 - \dfrac{9\sqrt{3}}{2\pi} + \dfrac{10}{\pi^2}$	$0.53223180\cdots$
3	$\dfrac{2\pi\sigma^3}{3}$	$5/8$	$\dfrac{219\sqrt{2}}{2240\pi} - \dfrac{89}{280} + \dfrac{4131}{2240\pi}\arctan\sqrt{2}$	$0.2869495\cdots$
4	$\dfrac{\pi^2\sigma^4}{4}$	$\dfrac{4}{3} - \dfrac{\sqrt{3}}{\pi}\dfrac{3}{2}$	$2 - \dfrac{27\sqrt{3}}{4\pi} + \dfrac{832}{45\pi^2}$ [17]	$0.15184606\cdots$
5	$\dfrac{4\pi^2\sigma^5}{15}$	$53/2^7$		0.07597 [18]
6	$\dfrac{\pi^3\sigma^6}{12}$	$\dfrac{4}{3} - \dfrac{\sqrt{3}}{\pi}\dfrac{9}{5}$	$2 - \dfrac{81\sqrt{3}}{10\pi} + \dfrac{38848}{1575\pi^2}$ [17]	$0.03336314\cdots$
7	$\dfrac{8\pi^3\sigma^7}{105}$	$289/2^{10}$		0.0098 [2]
8	$\dfrac{\pi^4\sigma^8}{945}$	$\dfrac{4}{3} - \dfrac{\sqrt{3}}{\pi}\dfrac{279}{140}$	$2 - \dfrac{2511\sqrt{3}}{280\pi} + \dfrac{17605024}{606375\pi^2}$ [17]	$-0.00255768\cdots$
9	$\dfrac{16\pi^4\sigma^9}{48}$	$6343/2^{15}$		-0.00841 [2]
10	$\dfrac{\pi^5\sigma^{10}}{240}$	$\dfrac{4}{3} - \dfrac{\sqrt{3}}{\pi}\dfrac{297}{140}$	$2 - \dfrac{2673\sqrt{3}}{280\pi} + \dfrac{49048616}{1528065\pi^2}$ [17]	$-0.01096248\cdots$
11	$\dfrac{32\pi^5\sigma^{11}}{10395}$	$35995/2^{18}$		
12	$\dfrac{\pi^6\sigma^{12}}{1440}$	$\dfrac{4}{3} - \dfrac{\sqrt{3}}{\pi}\dfrac{243}{110}$	$2 - \dfrac{2187\sqrt{3}}{220\pi} + \dfrac{11565604768}{337702365\pi^2}$ [17]	$-0.01067028\cdots$

convergence which is not on the positive real axis. If this radius is less than the freezing density then it will be impossible to reliably learn anything about the freezing transition from a knowledge of a finite number of virial coefficients.

It is thus most significant that the sixth and seventh virial coefficients for parallel hard cubes[40] were shown to be negative in 1962, and even more important that for an exactly solved hard squares model[41] and the hard hexagon model[42–44] the radius of convergence is limited by a singularity at complex density thus resulting in virial coefficients that oscillate in sign.

The purpose of this paper is to extend the results of Tables I and II and examine as closely as possible the question of whether or not the virial

coefficients B_k of the hard sphere gas in D dimensions have negative virial coefficients. The method we shall use is Monte-Carlo evaluations of the integrals in the Ree–Hoover expansion. In Section 2 we review the formalism of the Ree–Hoover expansion to establish our notation. In Section 3 we compute the virial coefficients B_5 and B_6 for dimensions up to $D = 50$. We find that B_5 is not monotonic but is in fact always positive. More importantly we find that B_6 is negative for all $D \geqslant 6$. Our numerical results are given in Table III. For higher virial coefficients the number of contributing diagrams rapidly increases. Consequently in this study we restrict our attention to various classes of diagrams which are studied in Section 4 where we are able to determine the class of diagrams which are dominant for large k. In Section 5 we use our results to form estimates of the radius of convergence to the virial series and we conclude in Section 6 with an evaluation of the various approximate equations of state for hard spheres.

Table III. Numerical Results for B_4/B_2^3, B_5/B_2^4, and B_6/B_2^5. The Underline Indicates the Position of the Local Minima and Maxima. Values for each Coefficient for $D = 3$, and for B_6 in $D = 4$, 5 Are Taken from Table I

D	B_4/B_2^3	B_5/B_2^4	B_6/B_2^5
3	$0.2869495\cdots$	$0.110252(1)$	$0.03881(6)$
4	$0.1518460\cdots$	$0.03565(5)$	$0.00769(3)$
5	$0.075978(4)$	$0.01297(1)$	$0.00094(3)$
6	$0.03336314\cdots$	$0.007528(8)$	$-0.00176(2)$
7	$0.009873(4)$	$\underline{0.007071(7)}$	$-0.00352(2)$
8	$-0.0025576\cdots$	$0.007429(6)$	$-0.00451(2)$
9	$-0.008575(3)$	$\underline{0.007438(6)}$	$\underline{-0.00478(1)}$
10	$-0.0109624\cdots$	$0.006969(5)$	$-0.00452(1)$
11	$\underline{-0.011334(3)}$	$0.006176(4)$	$-0.00395(1)$
12	$-0.0109624\cdots$	$0.005244(4)$	$-0.003261(7)$
13	$-0.009523(2)$	$0.004307(3)$	$-0.002580(6)$
14	$-0.008220(2)$	$0.003448(3)$	$-0.001975(4)$
15	$-0.006934(2)$	$0.002705(2)$	$-0.001472(3)$
20	$-0.0024621(7)$	$0.0006605(7)$	$-0.0002632(7)$
25	$-0.0007580(3)$	$0.0001348(2)$	$-3.72(1) \times 10^{-5}$
30	$-0.0002196(1)$	$2.515(6) \times 10^{-5}$	$-4.69(3) \times 10^{-6}$
35	$-6.162(3) \times 10^{-5}$	$4.47(1) \times 10^{-6}$	$-5.55(5) \times 10^{-7}$
40	$-1.697(1) \times 10^{-5}$	$7.69(3) \times 10^{-7}$	$-6.30(9) \times 10^{-8}$
45	$-4.618(4) \times 10^{-6}$	$1.298(7) \times 10^{-7}$	$-7.0(2) \times 10^{-9}$
50	$-1.247(1) \times 10^{-6}$	$2.16(1) \times 10^{-8}$	$-7.6(2) \times 10^{-10}$

2. REE–HOOVER EXPANSIONS

The original graphical expansion for the virial series is due to Mayer and Mayer,[45] in which each bond represents the function

$$f(\mathbf{r}) = \exp(-U(\mathbf{r})/k_B T) - 1 \tag{3}$$

where $\mathbf{r}$ is the distance between the two vertices. A useful re-summation was performed by Ree and Hoover[9, 46] by introducing the function

$$\tilde{f}(\mathbf{r}) = 1 + f(\mathbf{r}) = \exp(-U(\mathbf{r})/k_B T) \tag{4}$$

and then expanding each Mayer graph by substituting $1 = \tilde{f} - f$ for pairs of vertices not connected by f bonds. This method was previously used by Percus and Yevick[47] in comparing the exact values of the fourth and fifth virial coefficients with coefficients obtained from the Percus–Yevick equation, and by Percus[48] in discussing the derivation of the Percus–Yevick equation.

The fourth virial coefficient may then be written as

$$B_4 = -\frac{1}{8}\boxtimes - \frac{3}{4}\boxslash - \frac{3}{8}\square = \frac{1}{4}\varnothing - \frac{3}{8}\;\vdots\; = \frac{1}{4}\boxtimes - \frac{3}{8}\square \tag{5}$$

where the first expression is the expansion in Mayer graphs, the second is the expansion in Ree–Hoover graphs with the $\tilde{f}$ bonds indicated by dotted lines and the third shows the equivalent Ree–Hoover graphs with the f bonds indicated by solid lines. In the second expression the graph with no $\tilde{f}$ bonds is represented by $\varnothing$. In the case of hard spheres, the potential is given by Eq. (2) so $f(\mathbf{r})$ and $\tilde{f}(\mathbf{r})$ are particularly simple:

$$f(\mathbf{r}) = \begin{cases} -1 & |\mathbf{r}| < \sigma \\ 0 & |\mathbf{r}| > \sigma \end{cases} \tag{6}$$

$$\tilde{f}(\mathbf{r}) = \begin{cases} 0 & |\mathbf{r}| < \sigma \\ +1 & |\mathbf{r}| > \sigma \end{cases} \tag{7}$$

The virial coefficient B_k is given in terms of the Ree–Hoover diagrams of k points of which m are the end points of $\tilde{f}$ bonds $S_k[m, i]$ and a combinatorial factor $C_k[m, i]$ as

$$B_k = \sum_{m, i} B_k[m, i] \tag{8}$$

with

$$B_k[m, i] = C_k[m, i] \, S_k[m, i] \tag{9}$$

where the index i labels the graphs in the class with fixed k, m. The combinatorial factor is expressed as

$$C_k[m, i] = -\frac{k-1}{k!} \, s_k[m, i] \, \tilde{a}_k[m, i] \tag{10}$$

with

$$s_k[m, i] = k!/\sharp\text{Aut}\, S_k[m, i] \tag{11}$$

where $\sharp\text{Aut}\, S_k[m, i]$ is the cardinality of the automorphism group of the diagram $S_k[m, i]$ and $\tilde{a}_{m, l}[k]$ is the "star content" as defined by Ree and Hoover.[46] We will let $S_k[m, i]$ represent both the Ree–Hoover graph and the value of the corresponding integral. The k dependence of $C_k[m, i]$ is calculated by using the following relation for the star content.[46]

$$\tilde{a}_k[m, i] = (-1)^{k-1} \, (k-2) \, \tilde{a}_{k-1}[m, i] \tag{12}$$

The diagram $S_k[m, i]$ has $k-m$ points that are connected to all other points by f bonds and are therefore indistinguishable, leading to the relation

$$\sharp\text{Aut}\, S_k[m, i] = (k-m)! \, \sharp\text{Aut}\, S_m[m, i] \tag{13}$$

to obtain for $k > m$

$$C_k[m, i] = (-1)^{k(k-1)/2} \binom{k-1}{m-1} C_m[m, i] \tag{14}$$

where we note that for the complete star diagram $B_k[0, 1]$ we have $C_k[0, 1] = 1/k$.

For arbitrary D the number of Mayer graphs grows asymptotically as $k \to \infty$ as[49]

$$N(k) \sim \frac{2^{k(k-1)/2}}{k!} \tag{15}$$

However, when the Ree–Hoover transformation is made many diagrams have zero star content and hence do not contribute to the virial coefficient. From Table IV it appears that the ratio of contributing Ree–Hoover

Table IV. Number of Contributing Ree–Hoover and Mayer Diagrams as a Function of Order. The Number of Ree–Hoover Diagrams with Non-Zero Star Content for *k* = 9 Is a New Result, While the Other Values Are Taken from Refs. 9, 13, and 14

	Order							
	2	3	4	5	6	7	8	9
Mayer	1	1	3	10	56	468	7123	194066
RH	1	1	2	5	23	171	2606	81564
RH, $D=2$	1	1	2	4	15	78(66)		
RH/Mayer	1	1	0.667	0.500	0.410	0.365	0.366	0.420

diagrams to the number of Mayer diagrams is bounded below, and so it is reasonable to suppose that

$$\lim_{k \to \infty} N_{\mathrm{RH}}(k)/N(k) > 0 \qquad (16)$$

In addition Ree–Hoover graphs may be zero for geometrical reasons. The number of non-zero graphs for $D=2$ are taken from refs. 9 and 14, and listed in Table IV, where the value in parentheses excludes diagrams found to be negligible but which were not proven to be zero. For $D=1$ only one graph in the Ree–Hoover expansion is non-zero for each k, namely the complete star, but for $D \geqslant 2$ it is an open question as to how many non-zero graphs there are at order k.

2.1. Close Packed Diagrams

The $\tilde{f}$ graph form used by Ree and Hoover (e.g., in ref. 46) has the property that a single graph represents the sequence of diagrams $B_k[m, i]$ with m fixed where the $(k+1)$th order diagram is obtained from the kth by adding an additional point connected to all other points by an f bond. For example, all complete star diagrams of order k may be represented by the same symbol $\varnothing$. We call such graphs with $m < k$ close packed because no two points can be further apart than 2σ.

We find from Eq. (14) that the sign of $B_k[m, i]$ for fixed m, i is independent of k. We further obtain from Eq. (14) for k large and m, i fixed that

$$C_k[m, i] = C_m[m, i] \left(\frac{k^{m-1}}{(m-1)!} + O(k^{m-2}) \right) \qquad (17)$$

2.2. Loose Packed Diagrams

For diagrams in the class $B_k[k, i]$ there are no points which are connected to all other points by f bonds and therefore there exist sequences of diagrams which have the property that the size of the configuration grows as $k \to \infty$. We refer to this class of diagrams as "loose packed." For these graphs the f bond notation is more convenient.

The simplest loose packed diagram in $B_k[k, i]$ is the simple ring of k of the f bonds. We denote this diagram by the symbol R. More generally we consider graphs where a point is replaced by a diagram. We call such diagrams insertion diagrams and when we wish to make the type of insertion visually apparent we use the notation $R(\cdot)$ to represent a ring with a point replaced by a diagram. We also find it useful to label insertion diagrams by $R_{n,l}[k]$ where the index n is the number of points in the inserted diagram of k total points and l labels the diagrams with given k and n. All four and five point insertions were found by starting with all four and five point Mayer graphs, and adding an extra point that is connected to two points by f bonds. A canonical labeling for this graph was found using "nauty," a program due to B. McKay,[50] and matched with the five and six point graphs of Ree and Hoover[9] to find the star content. All insertions with non-zero star content are given in Table V along with the size of their automorphism group and over all combinatorial factor. From Eq. (14) we find the insertion diagrams have the alternating sign property that $(-1)^k R_{n,l}[k]$ has a sign which depends only on n and l but is independent of k.

Table V. Four and Five Point Insertions

Diagram	Label	Group size	Lowest order	$\tilde{a}_l[k]$	$C_k[k, i]$
R	R	$2k$	3	1	$-(k-1)/2k$
R($\diamond$)	$R_{4,1}$	4	6	1	$-(k-1)/4$
R($\diamond$)	$R_{4,2}$	4	5	-2	$(k-1)/2$
R($\bigcirc$)	$R_{5,1}$	2	8	1	$-(k-1)/2$
R($\diamond$)	$R_{5,2}$	12	7	1	$-(k-1)/12$
R($\diamond$)	$R_{5,3}$	4	7	-1	$(k-1)/4$
R($\diamond$)	$R_{5,4}$	1	7	-2	$2(k-1)$
R($\diamond$)	$R_{5,5}$	2	6	3	$-3(k-1)/2$
R($\diamond$)	$R_{5,6}$	4	7	-2	$(k-1)/2$
R($\diamond$)	$R_{5,7}$	2	6	1	$(k-1)/2$
R($\diamond$)	$R_{5,8}$	4	6	3	$-3(k-1)/4$
R($\diamond$)	$R_{5,9}$	12	6	-6	$(k-1)/2$

Table VI. Ree–Hoover Diagrams for B_4

Label	$s_k[m, i]$	$\tilde{a}_k[m, i]$	$C_k[m, i]$	$\tilde{f}$ form	f form	Insertion
$B_4[0, 1]$	1	-2	$2/8$	$\varnothing$	⊠	
$B_4[4, 1]$	3	1	$-3/8$	⋮⋮	□	R[4]

Multiple insertions are also possible when k is sufficiently large. We denote such a graph with n insertions as $R^{(m)}_{\{n_1, i_1\}, ..., \{n_m, i_m\}}$ where the subscripts indicate the types of insertions. For B_6 we see in Table VIII that there are three graphs which may be interpreted as being composed of two 4-point insertions.

We give in Tables VI–VIII the Ree–Hoover graphs and their associated combinatorial factors for $k = 4, 5, 6$. We here give both the representation of the graphs in terms of $\tilde{f}$ and f bonds. For the class of loose packed graphs in $B_k[k, i]$ we indicate the interpretation in terms of insertion diagrams with either multiple insertions or with a ring of one point and two bonds. In three cases the identification is not unique.

The labeling index i in $B_k[m, i]$ is chosen such that in $D = 2$ the magnitude of the contribution decreases with increasing i. If the diagram is identically zero for $D = 2$ then the ordering obtained from $D = 3$ is used when possible.

3. MONTE-CARLO CALCULATION OF B_k FOR $D \geqslant k - 1$

When $D \geqslant k - 1$ the integral $S_k[m, i]$ can be written in a form where the dimension D appears as a simple power in the integrand. Hence the Monte-Carlo procedure can simultaneously calculate the given Ree–Hoover diagram in an arbitrary set of dimensions, including non-integer values. The key advantage of this method over that of ref. 9 used in Section 4 is that we obtain fast convergence for high dimensions. We first present the details of the Monte-Carlo method and then the results for B_4, B_5, and B_6.

Table VII. Ree–Hoover Diagrams for B_5

Label	$s_k[m, i]$	$\tilde{a}_k[m, i]$	$C_k[m, i]$	$\tilde{f}$ form	f form	Insertion
$B_5[0, 1]$	1	-6	$6/30$	$\varnothing$	✪	
$B_5[4, 1]$	15	3	$-45/30$	⋮⋮	⬠	
$B_5[5, 1]$	30	-2	$60/30$	⌢	◈	$R_{4, 2}[5]$
$B_5[5, 2]$	12	1	$-12/30$	⬠	⬠	R[5]
$B_5[5, 3]$	10	1	$-10/30$	◠	◇	$R_{4, 1}[5]$

Table VIII. Ree–Hoover Diagrams for B_6. For Diagrams $B_6[6, 14]$, $B_6[6, 16]$, and $B_6[6, 17]$ the Assignment of Insertion Diagram Labels Is Not Unique and Both Possible Assignments Are Shown

Label	$s_k[m, i]$	$\tilde{a}_k[m, i]$	$C_k[m, i]$	$\tilde{f}$ form	f form	Insertion
$B_6[0, 1]$	1	24	$-24/144$	$\varnothing$	(diagram)	
$B_6[4, 1]$	45	-12	$540/144$	(diagram)	(diagram)	
$B_6[5, 1]$	180	8	$-1440/144$	(diagram)	(diagram)	
$B_6[5, 2]$	72	-4	$288/144$	(diagram)	(diagram)	
$B_6[5, 3]$	60	-4	$240/144$	(diagram)	(diagram)	
$B_6[6, 1]$	360	3	$-1080/144$	(diagram)	(diagram)	$R_{5,5}[6]$
$B_6[6, 2]$	180	-2	$360/144$	(diagram)	(diagram)	$R_{4,2}[6]$
$B_6[6, 3]$	60	1	$-60/144$	(diagram)	(diagram)	$R[6]$
$B_6[6, 4]$	60	-6	$360/144$	(diagram)	(diagram)	$R_{5,9}[6]$
$B_6[6, 5]$	180	-5	$900/144$	(diagram)	(diagram)	
$B_6[6, 6]$	90	-4	$360/144$	(diagram)	(diagram)	
$B_6[6, 7]$	45	4	$-180/144$	(diagram)	(diagram)	$R^{(2)}_{\{4,2\}\{4,2\}}[6]$
$B_6[6, 8]$	360	-1	$360/144$	(diagram)	(diagram)	
$B_6[6, 9]$	360	-2	$720/144$	(diagram)	(diagram)	$R_{5,4}[6]$
$B_6[6, 10]$	60	4	$-240/144$	(diagram)	(diagram)	
$B_6[6, 11]$	15	16	$-240/144$	(diagram)	(diagram)	
$B_6[6, 12]$	180	3	$-540/144$	(diagram)	(diagram)	$R_{5,8}[6]$
$B_6[6, 13]$	360	1	$360/144$	(diagram)	(diagram)	$R_{5,7}[6]$
$B_6[6, 14]$	90	-2	$180/144$	(diagram)	(diagram)	$R^{(2)}_{\{4,1\}\{4,2\}}[6]$ or $R_{5,6}[6]$
$B_6[6, 15]$	90	-1	$90/144$	(diagram)	(diagram)	$R_{5,3}[6]$
$B_6[6, 16]$	180	1	$-180/144$	(diagram)	(diagram)	$R_{4,1}[6]$ or $R_{5,1}[6]$
$B_6[6, 17]$	15	1	$-15/144$	(diagram)	(diagram)	$R^{(2)}_{\{4,1\}\{4,1\}}[6]$ or $R_{5,2}[6]$
$B_6[6, 18]$	10	4	$-40/144$	(diagram)	(diagram)	

We believe that all Ree–Hoover diagrams are non-zero for $D \geqslant k-1$ as it is possible to obtain a configuration for any diagram. We can see this by starting with a configuration where the distance between each point is exactly one, and then since each bond can be independently varied in length by a small amount we are able to satisfy the constraints imposed by f and $\tilde{f}$ bonds of any graph.

3.1. Monte-Carlo Method

In order to do the Monte-Carlo integration we need an appropriate measure for calculating Ree–Hoover diagrams in D-dimensional Euclidean

space, where we wish to integrate out coordinates to leave ourselves with the lowest dimensional integral possible. The integrand is a product of f and $\tilde{f}$ functions; for central potentials this leaves only the inter-particle distances as appropriate degrees of freedom. These form an independent set of $k(k-1)/2$ coordinates provided that $D \geqslant k-1$, where k is the order of the diagram and hence the number of points in the configuration. After taking the infinite volume limit, for an arbitrary diagram $S_k[m, i]$ we thus need to calculate integrals of the form

$$I = \int \prod_{i=1}^{k-1} d^D \mathbf{r_i} \, \mathbf{F}(r_{ij}) = \left(\prod_{i=1}^{k-1} \Omega_{D-i} \right) \int \prod_{i<j} da_{ij} [V(\{a_{ij}\})]^{D-k} \, \mathbf{F}(r_{ij}) \qquad (18)$$

where $\Omega_{D-1} \equiv 2\pi^{D/2}/\Gamma(D/2)$, $a_{ij} = |\mathbf{r_i} - \mathbf{r_j}|^2 = a_{ji}$, V is the volume of the parallel-piped defined by these distances in $\mathbb{R}^{k-1}$, and $\mathbf{F}(r_{ij})$ is an arbitrary function of the inter-particle distances. As shown for example in ref. 51, V may be expressed by the Cayley–Menger determinant:

$$V(\{a_i\}) = \left[\frac{(-1)^k}{2^{k-1}} \begin{vmatrix} 0 & 1 & 1 & 1 & \cdots & 1 \\ 1 & 0 & a_{12} & a_{13} & \cdots & a_{1k} \\ 1 & a_{21} & 0 & a_{23} & \cdots & a_{2k} \\ 1 & a_{31} & a_{32} & 0 & \cdots & a_{3k} \\ \vdots & \vdots & \vdots & \vdots & \ddots & \vdots \\ 1 & a_{k1} & a_{k2} & a_{k3} & \cdots & 0 \end{vmatrix} \right]^{\frac{1}{2}} \qquad (19)$$

An overall scale factor can be taken out of Eq. (19) by taking a_{12} to be the largest value, and then setting $a'_{ij} = a_{ij}/a_{12}$, so that

$$I = \frac{1}{2} k(k-1) \left(\prod_{i=1}^{k-1} \Omega_{D-i} \right) \int_0^\infty da_{12} \, a_{12}^{(k-1)D/2-1}$$

$$\times \left[\prod_{i<j\neq 2} \int_0^1 da'_{ij} \right] V(\{a_{12} \equiv 1, a'_{ij}\})^{D-k} \, \mathbf{F}(r_{ij}) \qquad (20)$$

A formula similar to Eq. (18) was previously obtained by Percus,[52] in which the integration of p vectors in dimension D is reduced to an integration of p vectors in p dimensions.

For the hard sphere fluid, the integrand is either zero or ± 1. In order to calculate $S_k[m, i]$ with m $\tilde{f}$ bonds and $[k(k-1)/2-m]$ f bonds, we may then proceed as follows. Generate a set of $[k(k-1)/2-1]$ values uniformly distributed between 0 and 1. Partition these values in two sets, where the largest $m-1$ values along with 1 represent $\tilde{f}$ bonds and the other

$[k(k-1)/2-m-1]$ values are f bonds, and then randomly assign these values to edges in the diagram. Check that these values of the edge lengths squared can be embedded as a simplex in $\mathbb{R}^{k-1}$, and if this is the case one can calculate the volume of the simplex and perform the a_{12} integral, making a contribution to the Monte-Carlo integral of

$$\frac{k}{D}(a_m^{-(k-1)D/2}-a_{m+1}^{-(k-1)D/2})\left(\prod_{i=1}^{k-1}\Omega_{D-i}\right)V(\{a_{12}\equiv 1, a_{ij}'\})^{D-k} \qquad (21)$$

where a_m and a_{m+1} are the mth and $(m+1)$th largest values of a_{ij} respectively.

We have used this procedure to compute B_4, B_5, and B_6. For B_4 and B_5 500 batches of 5×10^6 configurations were used, while for B_6 20 batches of 2×10^9 configurations were generated. Uncertainties were calculated using

$$\text{Error}=\left[\sum_{j=1}^{q}\frac{(\langle I_j\rangle-\langle I\rangle)^2}{q(q-1)}\right]^{\frac{1}{2}} \qquad (22)$$

where there are q independent batches with value I_j.

3.2. Results

The values of the individual contributions $B_k[m, i]$ to the virial coefficients B_k for $k = 4, 5, 6$ are given in Appendix A in Tables XII–XIV, for many values of $D \leqslant 50$. The values of the virial coefficients B_k/B_2^{k-1} for $D \leqslant 50$ are given in Table III.

The most important feature of the virial coefficients in Table III are the sign changes in B_4 and B_6. A previous estimate for the dimension at which B_4 becomes negative of $D \approx 7.8$ was obtained by Luban and Baram[16] by means of a linear interpolation of the results of Ree and Hoover,[2] and also by an independent calculation. We further note the local minimum at in B_5 which confirms the tentative prediction of Loeser et al.[53] To obtain accurate values for these zeros, minima and maxima as a function of D the data were fitted with cubic splines. All of these values are summarized in Table IX. Note that the error estimates were made by fitting, for example, $B_4 + \Delta B_4$ and $B_4 - \Delta B_4$ with cubic splines to obtain a confidence interval for where B_4 becomes negative. A least squares fit was not used because the error in values at different dimensions are not independent, as they are calculated simultaneously and not as independent samples.

Table IX. Maxima and Minima for B_4/B_2^3, B_5/B_2^4, and B_6/B_2^5

B_4/B_2^3	B_5/B_2^4	B_6/B_2^5
Becomes negative	Local minimum	Becomes negative
$D_4^{\text{neg}} = 7.7320(4)$	$D = 6.87$	$D_6^{\text{neg}} = 5.30(2)$
Local minimum	Local maximum	Local minimum
$D = 10.7583(2)$	$D = 8.31$	$D = 8.942(2)$

It is most important that B_6 becomes negative at a lower dimension than B_4. If this trend continues, we may expect that for B_{2k} the dimension at which the coefficient becomes negative will decrease for higher orders and it is not unreasonable to expect that B_8 will be negative for $D = 5$ and possibly even $D = 4$. In addition, even though B_5 is always positive, the existence of a local minimum at $D = 6.87$ shows that the increasing number of contributing diagrams results in more complex dimensional dependence.

To obtain further insight into the structure of the virial coefficients we examine the individual contributions in Tables XII–XIV. There we see by examining the dependence of the contributions on D that by the time $D = 50$ the Ree–Hoover ring diagram R is several orders of magnitude greater than all other diagrams. We therefore make the following conjecture:

Conjecture 1.

$$\lim_{D \to \infty} B_k(D)/\mathsf{R}(D) = 1 \qquad (23)$$

In particular it follows from this conjecture that for each k

$$(-1)^{k-1} B_k(D) > 0 \qquad \text{for sufficiently large } D \qquad (24)$$

A similar conjecture in terms of Mayer diagrams was made by Frisch and Percus[54] in the course of their examination of Mayer diagrams at high dimensionality.

We find further for $D = 50$ that not only does the Ree–Hoover ring diagram dominate but that the largest diagram in each $B_k[m, i]$ has property that if $m > m'$ then

$$B_k[m, i]_{\max} \gg B_k[m', i]_{\max} \qquad (25)$$

We refer to this ordering as the principle of "loose packed dominance."

We also note that within the loose packed class $B_k[k, i]$ that the ordering of the magnitude of the diagrams at $D = 2$ and at $D = 50$ is drastically different. For example we note that the diagram $\mathsf{R}_{4,1}$ which vanishes

identically in $D = 2$ is the second largest diagram for $D = 50$. More generally we find for $D = 50$ that the contributions in $B_6[6, i]$ are ordered in magnitude as

$$\mathsf{R} > \mathsf{R}_{4,1} > \mathsf{R}_{4,2} > \mathsf{R}_{5,4} > \mathsf{R}_{5,5} > \mathsf{R}_{5,3} > \mathsf{R}_{5,2} = \mathsf{R}^{(2)}_{\{4,1\},\{4,1\}} \qquad (26)$$

where we use the labeling of insertion diagrams in Tables V and VIII. We make the observation that these insertion diagrams are the largest in the class $B_k[k, i]$, and refer to this as "insertion graph dominance."

4. MONTE-CARLO CALCULATION OF HIGH ORDER DIAGRAMS

The observation and conjecture of the dominance of the Ree–Hoover ring diagram at large dimensions demonstrates that negative virial coefficients in the hard sphere fluids is a common occurrence. However it says nothing about the minimum dimension at which the coefficient B_k will become negative for fixed k nor does it give any indication of whether or not virial coefficients of odd order can ever be negative. Ideally this question should be studied by computing further viral coefficients beyond those in Table I for large k. Here we will begin this program by examining selected classes of diagrams $B_k[m, i]$ for values of k up to 17. In particular we examine the conjecture that the features of loose packed dominance and insertion graph dominance found for large D and fixed k holds also for fixed D and large k.

4.1. Method

The Monte-Carlo procedure used for this study is the same as that used by Ree and Hoover (e.g., in ref. 9). Random configurations are generated by placing one point at the origin of some arbitrary coordinate system, then the next is randomly placed within a D-dimensional unit sphere centered on the first point, and so on. The final configuration is then tested to see if it satisfies the requirements imposed on distances by the diagram being calculated. For each diagram we used batches of 10^6 configurations, with enough batches to give accuracy better than two percent up to a maximum of 10000 batches, and errors were calculated using Eq. (22).

4.2. Results

The evaluations of the following diagrams are presented in Tables XV–XXII of Appendix B for values of k up to 17 and values of D up to 7;

Table X.   Largest Diagrams

	Dimension						
k	1	2	3	4	5	6	∞
4	$\varnothing$	$\varnothing$	$\varnothing$	$\varnothing$	$\varnothing$	$\varnothing$	R
5	$\varnothing$	$\varnothing$	$\varnothing$	$\varnothing$	$\varnothing$	R	R
6	$\varnothing$	$\varnothing$	$\varnothing$	$\varnothing$	R	R	R
7	$\varnothing$	$\varnothing$	$\varnothing$	R	R	R	R
8	$\varnothing$	$\varnothing$	R($\diamondsuit$)	R	R	R	R
9	$\varnothing$	$\varnothing$	R($\diamondsuit$)	R($\diamondsuit$)	R	R	R
10	$\varnothing$	$\varnothing$	R($\diamondsuit$)	R($\diamondsuit$)	R		R
11	$\varnothing$	$\varnothing$	R($\diamondsuit$)	R($\diamondsuit$)	R		R
12	$\varnothing$	$\varnothing$	R($\diamondsuit$)	R($\diamondsuit$)	R($\diamondsuit$)		R
13	$\varnothing$	$\varnothing$	R($\diamondsuit$)	R($\diamondsuit$)	R($\diamondsuit$)		R
14	$\varnothing$		R($\diamondsuit$)	R($\diamondsuit$)	R($\diamondsuit$)		R
15	$\varnothing$		R($\diamondsuit$)	R($\diamondsuit$)	R($\diamondsuit$)		R

$B_k[0, 1]$, $B_k[4, 1]$, $B_k[5, 1]$, R$[k]$, R$_{4, 2}[k]$, R$_{4, 1}[k]$, R$_{5, 5}[k]$, and the "pin-wheel diagram" in $B_k[k-1, 1]$ obtained by adding one point which is connected by f bonds to all points in the Ree–Hoover ring R$[k-1]$. We note that for $k = 5$ the pinwheel is $B_5[4, 1]$ and for $k = 6$ it is $B_6[5, 2]$.

To investigate the conjecture of loose packed dominance for fixed D and large k we use the tables of Appendix B to find for each k and D which diagram of this set is the largest. This is shown in Table X. We also use Tables XV and XVIII to compute the ratio R$/B_k[0, 1]$, and display the results in Table XI. From this table we see that for $D \geqslant 3$ that the Ree–Hoover ring R quickly dominates the complete star diagram as k increases. However, for $D = 2$, even though the ratios are monotonically increasing for $k \geqslant 6$ the ring has not dominated the complete star at $k = 17$. If we extrapolate the increasing ratios in Table XI for $D = 2$ we can esti-mate that the ring will be larger for approximately $k \sim 22$.

Further information is obtained from the ratios of $B_k[4, 1]/B_k[0, 1]$ and $B_k[5, 1]/B_k[0, 1]$ plotted in Figs. 1 and 2 of Appendix C. In these figures it is seen that the ratios $B_k[4, 1]/B_k[0, 1]$ and $B_k[5, 1]/B_k[0, 1]$ increase linearly with k. Thus while for the values of k studied the ratios only rarely exceed one it appears that if we extrapolate to sufficiently large k that the inequalities in Eq. (25) will be satisfied for $m, m' = 0, 4, 5$.

The relative size of diagrams in the class $B_k[k, i]$ and $B_k[k-1, i]$ is studied by comparing the Ree–Hoover ring diagram R$[k]$ of Table XVIII with the corresponding pinwheel diagram of Table XXII. It is clear that in each dimension that for sufficiently large k the pinwheel diagram will

Table XI. R/$\varnothing$

k	$D = 2$	$D = 3$	$D = 4$	$D = 5$	$D = 6$
4	$-0.0299(2)$	$-0.0942(4)$	$-0.1964(8)$	$-0.3405(7)$	$-0.535(2)$
5	$0.0238(2)$	$0.1143(7)$	$0.362(3)$	$0.911(6)$	$1.97(1)$
6	$-0.0230(4)$	$-0.184(2)$	$-0.91(1)$	$-3.47(5)$	$-11.7(2)$
7	$0.0237(5)$	$0.337(7)$	$2.92(6)$	$18.8(5)$	$85(2)$
8	$-0.0277(6)$	$-0.73(2)$	$-10.4(3)$	$-100(3)$	$-780(30)$
9	$0.0350(8)$	$1.67(5)$	$44(1)$	$710(30)$	$11000(2000)$
10	$-0.043(1)$	$-4.1(1)$	$-177(7)$	$-5100(800)$	
11	$0.056(2)$	$10.3(3)$	$860(80)$		
12	$-0.076(2)$	$-26.0(7)$	$-3000(800)$		
13	$0.102(3)$	$60(5)$			
14	$-0.133(5)$	$-160(30)$			
15	$0.18(1)$				
16	$-0.24(2)$				
17	$0.39(5)$				

vanish, and although this can't be shown numerically one can see the ratio of the pinwheel to the ring R[k] decreases rapidly as k increases.

We conclude this discussion of results by examining the relative magnitudes of insertion diagrams in $B_k[k, i]$. In Figs. 3–5 of Appendix C we plot the ratios $R_{4,2}/R$, $R_{4,1}/R$, and $R_{5,5}/R$ as a function of k for various D. We see that for sufficiently large k all three ratios have a linear increase with respect to k. We also note that even though the ratio $R_{4,1}/R_{4,2}$ is small in low dimensions, it approaches a non-zero constant as $k \to \infty$, and for sufficiently large D the ratio is in fact greater that unity.

The examination of all available data supports the following conjectures.

Conjecture 2.   The loose packed diagrams in $B_k[k, i]$ dominate all other diagrams for large k when $D \geqslant 3$.

In connection with this conjecture we note that the three largest diagrams for B_6 in $D = 5, 6$ are $R_{5,5}$, $R_{4,1}$, and R and that the sum of these three largest diagrams shares the property with B_6 itself of changing sign between $D = 5$ and $D = 6$. We restrict the conjecture to dimensions $D \geqslant 3$ because at this stage there is not yet enough data to support the case for $D = 2$.

Conjecture 3.   The insertion diagrams all have the same exponential rate of growth as the Ree–Hoover ring.

5. ESTIMATES OF THE RADIUS OF CONVERGENCE

The dominance of loose packed diagrams for fixed $D \geqslant 3$ and large k may be used to discuss the question of sign change in the virial coefficients and the radius of convergence of the virial expansion. Of greatest importance is the relation of the radius of convergence to the packing fractions η_f at which freezing occurs which have been numerically determined as $\eta_f = 0.49$ in $D = 3$,[24, 35] $\eta_f = 0.31$ in $D = 4$, and $\eta_f = 0.19$ in $D = 5$ as obtained from ref. 55 and 56.

It may be that there are sequences of loose packed diagrams that grow faster than the ring, but for low order the largest diagrams can be characterized as insertion diagrams and these appear to have the same exponential rate of growth as the ring. Hence we will concentrate on the Ree–Hoover ring R. We first note that the absolute value of this diagram must be strictly less than the absolute value of the corresponding Mayer diagram where all $\tilde{f}$ bonds are replaced by unity. The resulting Mayer ring diagram has been long ago evaluated[57] in terms of Bessel functions of the first kind $J_{D/2}(x)$ and thus we obtain

$$(-1)^{k-1} \mathsf{R}[k]/B_2^{k-1} \leqslant \frac{(k-1)(2\pi)^{kD/2}}{2k\Omega_{D-1}^{k-2}} \int_0^\infty dx\, x^{D-1} \left[\frac{J_{D/2}(x)}{x^{D/2}} \right]^k \qquad (27)$$

The large k behavior of this integral is easily obtained by steepest descents by noting that the maximum value of $J_{D/2}(x)/x^{D/2}$ occurs at $x = 0$. Thus we have as $k \to \infty$

$$(-1)^{k-1} \mathsf{R}[k]/B_2^{k-1} \leqslant \frac{(k-1)(1+D/2)^{D/2}}{k^{1+D/2}\Gamma(1+D/2)} 2^{k-2} \qquad (28)$$

and hence $\mathsf{R}[k]$ satisfies the bound

$$|\mathsf{R}[k+1]/(B_2\mathsf{R}[k])| \leqslant 2 \qquad (29)$$

This leads to a packing fraction at the radius of convergence of the sum of Ree–Hoover diagrams of $\eta_{\mathrm{rh}} = 2^{-D}$ which is substantially greater than the lower bound $0.145/2^D$ of Lebowitz and Penrose[58] but which is still much smaller than the freezing densities η_f. This value of η_{rh} is of the same order of magnitude as the lower bounds on the termination density due to Baram and Fixman[59] which are $\eta_t > 0.25838$ for $D = 2$ and $\eta_t > 0.12681$ for $D = 3$. This is compatible with the pressure being analytic for positive values of η less than η_f because the alternations of sign of $\mathsf{R}[k]$ puts the leading singularity on the negative η axis.

However the ratios $|R[k+1]/(B_2 R[k])|$ obtained from Table XVIII are substantially below the bound Eq. (29). In fact we see from each $D \geqslant 4$ that there is some value of k such that for all greater values of k the values of R/B_2^{k-1} increase. The order k must surely be greater than this value before it can be claimed that the asymptotic regions has been achieved. If we use that maximum ratios as obtained from Table XVIII we estimate that for $D = 4$ we have $\eta_{\rm rh} \sim 0.12$ and for $D = 5$ we have $\eta_{\rm rh} \sim 0.052$. In $D = 3$ if we assume that the data of Table XVIII extrapolates to a constant as $k \to \infty$ then the radius of convergence of the Ree–Hoover ring is $\eta_{\rm rh} = 0.25$. At most the ratios are bounded below by 0.91 which leads to $\eta_{\rm rh} = 0.27$. All of these estimated radii of convergence are substantially less than the freezing densities $\eta_{\rm f}$.

In order for the radius of convergence of the virial series to be larger than these estimates obtained from the Ree–Hoover ring there must be cancellations between diagrams in the class $B_k[k, i]$. Such cancellations can occur because, for example, the diagrams $R_{4,2}[k]$ and $R_{5,5}[k]$ which have magnitudes comparable to $R[k]$ have signs opposite to $R[k]$. Furthermore from Table I we see that B_k is indeed less in magnitude than $R[k]$ for $k = 6, 7, 8$. What cannot be inferred from the existing data is whether or not when k is sufficiently large that the diagrams are in their asymptotic region that the cancellation is severe enough to reduce the exponential rate of growth of the ratios B_{k+1}/B_k. Unless the cancellation becomes sufficiently great for the radius of convergence to be larger than the freezing density then the leading singularity cannot be on the real η axis and there must be oscillation in the signs of the virial coefficients.

6. APPROXIMATE EQUATIONS OF STATE FOR HARD SPHERES

For over 40 years the eight virial coefficients of Table I have been used to inspire many approximate equations of state for the low density phase of hard spheres. These approximates may be grouped by the location of their leading singularity into the following three classes:

1. High Order Poles at $\eta = 1$

Examples of these are the proposals of Thiele[19]

$$Pv/k_B T = \frac{1 + 2\eta + 3\eta^2}{(1 - \eta)^2} \tag{30}$$

Reiss, Frisch, and Lebowitz,[60] and Wertheim[20]

$$Pv/k_B T = \frac{1 + \eta + \eta^2}{(1 - \eta)^3} \tag{31}$$

Guggenheim[22]

$$Pv/k_BT = \frac{1}{(1-\eta)^4} \tag{32}$$

and the proposal of Carnahan and Starling[23]

$$Pv/k_BT = \frac{1+\eta+\eta^2-\eta^3}{(1-\eta)^3} \tag{33}$$

We do note that Torquato[32, 33] proposes an equation of state which agrees with Eq. (33) for $\eta < \eta_f$ but which is of a different form for $\eta > \eta_f$.

2. Simple Poles at[25, 26] or Near the Packing Fraction $\eta_{cp} = 0.74048\cdots$ of Closest Packed Hard Spheres[9, 13, 24, 31]

In particular the Padé analysis made in ref. 13 has simple poles at

$$\eta = (1.22 \pm 0.09i)\, \eta_{cp} \tag{34}$$

which leads to sign oscillations beginning with B_{45}.

3. A Fractional Power Law Divergence at or Near the "Random Close Packed" Density $\eta_{rcp} = 0.64$ as Defined by Refs. 61–64

These approximates are obtained from a D-log Padé analysis and are (generalizations) of the form

$$Pv/k_BT = A(\eta - \eta_{rcp})^{-s} \tag{35}$$

As an example s is estimated as 1 in ref. 27, as 0.678 in ref. 28, and 0.76 in ref. 30. In ref. 29 other values of η_{rcp} are chosen and the values of s lie in the range $0.6 \leqslant s \leqslant 0.9$ depending on the approximation used.

All these approximate equations of state share the feature that their leading singularity is at a value of η which is greater than the freezing density $\eta_f = 0.49$ and indeed is even greater than the solid end of the phase transition $\eta_s = 0.542$. This fact has lead to the assumption that the virial expansion is analytic at the freezing transition η_f and this qualitative feature is incorporated into most of the phenomenological theories used to describe freezing.[36–39] It is therefore of great importance that the estimates of the radius of convergence made above on the basis of loose packed dominance and the assumption of no cancellation estimated the radius of convergence at no more than 0.27.

The estimate of the radius of convergence relies on values of k beyond the first eight virial coefficients used to obtain the approximate equations of state. Therefore it is fair to say that none of the approximates incorporates the true large k behavior of the virial coefficients. Thus even if there is cancellation for large k for the set of close packed diagrams none of the approximates is based on computations which can observe these cancellations and hence no known approximate equation of state can be considered reliable. We therefore conclude that at present there exists no evidence to support the claim that the virial expansion has a radius of convergence greater than the freezing density η_f.

APPENDIX A. INDIVIDUAL DIAGRAM CONTRIBUTIONS FOR B_4, B_5, AND B_6

In this appendix we tabulate the contributions of the individual Ree–Hoover diagrams to the virial coefficients for B_4, B_5, and B_6.

Table XII.   Individual Diagram Contributions to B_4

D	$B_4[0, 1]/B_2^3$	$B_4[4, 1] B_2^3$	B_4/B_2^3
3	$0.31673(2)$	$-0.029781(8)$	$0.2869495\cdots$
4	$0.1888655\cdots$	$-0.0370195\cdots$	$0.1518460\cdots$
5	$0.115211(3)$	$-0.039233(3)$	$0.075978(4)$
6	$0.0714700\cdots$	$-0.0381069\cdots$	$0.03336314\cdots$
7	$0.044927(2)$	$-0.035055(3)$	$0.009873(3)$
7.7	$0.032669(2)$	$-0.032331(3)$	$0.000338(3)$
7.8	$0.031227(2)$	$-0.031920(3)$	$-0.000693(3)$
8	$0.0285344\cdots$	$-0.0310921\cdots$	$-0.0025576\cdots$
9	$0.018286(1)$	$-0.026861(3)$	$-0.008575(3)$
10	$0.0117986\cdots$	$-0.0227611\cdots$	$-0.0109624\cdots$
11	$0.0076638(8)$	$-0.018997(3)$	$-0.011333(3)$
12	$0.0050018\cdots$	$-0.0156721\cdots$	$-0.0109624\cdots$
13	$0.0032819(5)$	$-0.012805(2)$	$-0.009523(2)$
14	$0.0021615(4)$	$-0.010381(2)$	$-0.008220(2)$
15	$0.0014288(3)$	$-0.008362(2)$	$-0.006933(2)$
20	$0.00018830(6)$	$-0.0026504(7)$	$-0.0024621(7)$
25	$0.00002615(1)$	$-0.0007841(3)$	$-0.0007580(3)$
30	$3.763(3) \times 10^{-6}$	$-0.0002233(1)$	$-0.0002196(1)$
35	$5.560(7) \times 10^{-7}$	$-0.00006217(3)$	$-0.00006162(3)$
40	$8.38(1) \times 10^{-8}$	$-0.00001705(1)$	$-0.00001697(1)$
45	$1.284(3) \times 10^{-8}$	$-4.631(4) \times 10^{-6}$	$-4.618(4) \times 10^{-6}$
50	$1.992(5) \times 10^{-9}$	$-1.249(1) \times 10^{-6}$	$-1.247(1) \times 10^{-6}$

Table XIII. Individual Diagram Contributions to B_5. Values for Discs and Spheres Taken from Ref. 9. The Contributions from the Ree–Hoover Ring Diagram $B_5[5, 2]$ Are Underlined

	discs	spheres	$D = 4$	$D = 5$
B_5/B_2^4	0.3336	0.1103	0.03565(5)	0.01297(1)
$B_5[0, 1]/B_2^4$	0.3618	0.1422	0.059015(9)	0.025442(1)
$B_5[4, 1]/B_2^4$	-0.0266	-0.0314	$-0.02650(2)$	$-0.019184(5)$
$B_5[5, 1]/B_2^4$	-0.0102	-0.0165	$-0.01762(4)$	$-0.015511(4)$
$B_5[5, 2]/B_2^4$	<u>0.0086</u>	<u>0.0162</u>	<u>0.02131(2)</u>	<u>0.022980(7)</u>
$B_5[5, 3]/B_2^4$	0	-0.0002	$-0.0005498(5)$	$-0.0007622(3)$
	$D = 6$	$D = 7$	$D = 8$	$D = 50$
B_5/B_2^4	0.007528(8)	0.007071(7)	0.007429(6)	$2.17(1) \times 10^{-8}$
$B_5[0, 1]/B_2^4$	0.0112852(7)	0.0051189(4)	0.0023640(3)	$1.67(8) \times 10^{-15}$
$B_5[4, 1]/B_2^4$	$-0.012899(4)$	$-0.008296(3)$	$-0.005185(2)$	$-6.1(1) \times 10^{-13}$
$B_5[5, 1]/B_2^4$	$-0.012351(3)$	$-0.009220(3)$	$-0.006588(3)$	$-1.38(3) \times 10^{-11}$
$B_5[5, 2]/B_2^4$	<u>0.022332(6)</u>	<u>0.020277(6)</u>	<u>0.017522(6)</u>	<u>$2.17(1) \times 10^{-8}$</u>
$B_5[5, 3]/B_2^4$	$-0.0008395(4)$	$-0.0008090(4)$	$-0.0007149(4)$	$-4.84(7) \times 10^{-11}$

Table XIV. Individual Diagram Contributions to B_6. Values for Discs and Spheres Taken from Ref. 9. The Contributions from the Ree–Hoover Ring Diagram $B_6[6, 3]$ Are Underlined. For *D* = 50 When the Value *x.xx* × 10^m Has $m \leqslant -16$ We Write $\sim 10^m$

	discs	spheres	$D = 5$	$D = 6$
B_6/B_2^5	0.1994	0.0386	0.00102(8)	$-0.00176(2)$
$B_6[0, 1]/B_2^5$	0.2292	0.0588	0.0048248(9)	0.0014771(1)
$B_6[4, 1]/B_2^5$	-0.0273	-0.0212	$-0.00569(2)$	$-0.002600(3)$
$B_6[5, 1]/B_2^5$	-0.0191	-0.0187	$-0.00719(1)$	$-0.003800(4)$
$B_6[5, 2]/B_2^5$	0.0090	0.0099	0.00498(2)	0.003038(4)
$B_6[5, 3]/B_2^5$	0	-0.0002	$-0.000244(1)$	$-0.0001759(3)$
$B_6[6, 1]/B_2^5$	0.0088	0.0132	0.01029(4)	0.00735(1)
$B_6[6, 2]/B_2^5$	0.0077	0.0121	0.01064(4)	0.008204(8)
$B_6[6, 3]/B_2^5$	<u>-0.0051</u>	<u>-0.0109</u>	<u>$-0.01702(5)$</u>	<u>$-0.01693(2)$</u>
$B_6[6, 4]/B_2^5$	-0.0019	-0.0027	$-0.001520(4)$	$-0.0009332(8)$
$B_6[6, 5]/B_2^5$	-0.0010	-0.0022	$-0.001559(9)$	$-0.001001(2)$
$B_6[6, 6]/B_2^5$	-0.0009	-0.0011	$-0.000553(1)$	$-0.0003335(3)$
$B_6[6, 7]/B_2^5$	-0.0005	-0.0007	$-0.000437(1)$	$-0.0002948(3)$
$B_6[6, 8]/B_2^5$	0.0004	0.0008	0.000712(2)	0.0004958(8)
$B_6[6, 9]/B_2^5$	0.0001	0.0012	0.00256(2)	0.002356(7)

Table XIV. *(Continued)*

	discs	spheres	$D = 5$	$D = 6$
$B_6[6, 10]/B_2^5$	0.0000	0.0002	0.0003086(8)	0.0002481(2)
$B_6[6, 11]/B_2^5$	-0.0000	-0.0003	$-0.0002596(7)$	$-0.0001587(1)$
$B_6[6, 12]/B_2^5$	0	-0.0002	$-0.000472(2)$	$-0.0003931(6)$
$B_6[6, 13]/B_2^5$	0	0.0002	0.000318(4)	0.000285(1)
$B_6[6, 14]/B_2^5$	0	-0.0000	$-0.0000991(5)$	$-0.0001007(2)$
$B_6[6, 15]/B_2^5$	0	0.0000	0.000046(2)	0.0000486(9)
$B_6[6, 16]/B_2^5$	0	0.0004	0.00138(1)	0.001463(2)
$B_6[6, 17]/B_2^5$	0	$-0?$	$-2.00(1) \times 10^{-6}$	$-3.176(6) \times 10^{-6}$
$B_6[6, 18]/B_2^5$	0	0	$2.59(1) \times 10^{-7}$	$3.696(8) \times 10^{-7}$

	$D = 7$	$D = 8$	$D = 50$
B_6/B_2^5	$-0.00352(2)$	$-0.00451(1)$	$-7.6(2) \times 10^{-10}$
$B_6[0, 1]/B_2^5$	0.00046725(4)	0.00015174(2)	$\sim 10^{-22}$
$B_6[4, 1]/B_2^5$	$-0.001145(1)$	$-0.0004946(6)$	$\sim 10^{-20}$
$B_6[5, 1]/B_2^5$	$-0.001902(2)$	$-0.0009209(9)$	$\sim 10^{-18}$
$B_6[5, 2]/B_2^5$	0.001752(2)	0.0009748(9)	$\sim 10^{-16}$
$B_6[5, 3]/B_2^5$	$-0.0001124(2)$	$-0.0000665(1)$	$\sim 10^{-18}$
$B_6[6, 1]/B_2^5$	0.004866(6)	0.003063(3)	$6.7(7) \times 10^{-15}$
$B_6[6, 2]/B_2^5$	0.005887(5)	0.004019(3)	$1.6(1) \times 10^{-13}$
$B_6[6, 3]/B_2^5$	$\underline{-0.01540(2)}$	$\underline{-0.01318(2)}$	$\underline{-7.6(2) \times 10^{-10}}$
$B_6[6, 4]/B_2^5$	$-0.0005349(5)$	$-0.0002926(3)$	$\sim 10^{-18}$
$B_6[6, 5]/B_2^5$	$-0.000589(1)$	$-0.0003277(6)$	$\sim 10^{-18}$
$B_6[6, 6]/B_2^5$	$-0.0001883(1)$	$-0.00010175(8)$	$\sim 10^{-18}$
$B_6[6, 7]/B_2^5$	$-0.0001858(2)$	$-0.0001114(2)$	$\sim 10^{-17}$
$B_6[6, 8]/B_2^5$	0.0003158(4)	0.0001895(2)	$\sim 10^{-17}$
$B_6[6, 9]/B_2^5$	0.001912(4)	0.001428(3)	$5.3(5) \times 10^{-14}$
$B_6[6, 10]/B_2^5$	0.0001778(1)	0.0001180(1)	$\sim 10^{-16}$
$B_6[6, 11]/B_2^5$	$-0.00008782(7)$	$-0.00004567(4)$	$\sim 10^{-20}$
$B_6[6, 12]/B_2^5$	$-0.0002848(4)$	$-0.0001889(2)$	$\sim 10^{-17}$
$B_6[6, 13]/B_2^5$	0.0002231(6)	0.0001595(4)	$\sim 10^{-16}$
$B_6[6, 14]/B_2^5$	$-0.0000868(2)$	$-0.0000671(1)$	$\sim 10^{-16}$
$B_6[6, 15]/B_2^5$	0.0000447(4)	0.0000371(3)	$2.2(3) \times 10^{-15}$
$B_6[6, 16]/B_2^5$	0.001358(2)	0.001147(2)	$1.34(8) \times 10^{-12}$
$B_6[6, 17]/B_2^5$	$-3.774(8) \times 10^{-6}$	$-3.758(9) \times 10^{-6}$	$-1.5(1) \times 10^{-15}$
$B_6[6, 18]/B_2^5$	$3.944(9) \times 10^{-7}$	$3.524(9) \times 10^{-7}$	$\sim 10^{-18}$

APPENDIX B. NUMERICAL VALUES OF SELECTED DIAGRAMS TO HIGH ORDER

In this appendix we tabulate the results of Monte-Carlo evaluations of selected diagrams $B_k[m, i]$ to orders up to $k = 17$.

Table XV. $\varnothing/B_2^{k-1} = B_k[0, 1]/B_2^{k-1}$

k	$D = 2$	$D = 3$	$D = 4$	$D = 5$	$D = 6$
3	0.7821(1)	0.6248(2)	0.5063(2)	0.4143(2)	0.3410(2)
4	0.5488(4)	0.3166(3)	0.1888(2)	0.1153(2)	0.0713(2)
5	0.3620(3)	0.1420(2)	0.0591(2)	0.02522(8)	0.01121(7)
6	0.2292(3)	0.0593(2)	0.01648(6)	0.00487(6)	0.00148(2)
7	0.1412(3)	0.0233(2)	0.00424(6)	0.00076(1)	0.000170(3)
8	0.0844(4)	0.0087(2)	0.00101(2)	0.000129(3)	$1.81(5) \times 10^{-5}$
9	0.0505(4)	0.00315(6)	0.000226(5)	$1.78(7) \times 10^{-5}$	$1.3(2) \times 10^{-6}$
10	0.0293(4)	0.00111(2)	$5.2(2) \times 10^{-5}$	$2.5(4) \times 10^{-6}$	
11	0.0170(3)	0.000380(8)	$1.0(1) \times 10^{-5}$		
12	0.0097(2)	0.000128(3)	$2.7(7) \times 10^{-6}$		
13	0.0053(1)	$5.2(4) \times 10^{-5}$			
14	0.00304(6)	$1.7(3) \times 10^{-5}$			
15	0.00179(4)				
16	0.00098(2)				
17	0.00055(1)				

Table XVI. $/B_2^{k-1} = B_k[4, 1]/B_2^{k-1}$

k	$D = 2$	$D = 3$	$D = 4$	$D = 5$	$D = 6$
4	−0.01644(5)	−0.02981(9)	−0.0370(1)	−0.0391(1)	−0.0382(1)
5	−0.0264(3)	−0.0316(2)	−0.0270(2)	−0.0189(2)	−0.0130(2)
6	−0.0285(5)	−0.0219(4)	−0.0117(2)	−0.0059(1)	−0.00256(5)
7	−0.0239(5)	−0.0114(2)	−0.00403(8)	−0.00130(3)	−0.00039(1)
8	−0.0183(4)	−0.0056(1)	−0.00120(5)		
9	−0.0123(3)	−0.0025(1)			
10	−0.0086(4)				
11	−0.0056(2)				
12	−0.0038(2)				
13	−0.0023(3)				

Table XVII. $\frown /B_2^{k-1} = B_k[5, 1]/B_2^{k-1}$

k	$D = 2$	$D = 3$	$D = 4$	$D = 5$	$D = 6$
5	$-0.01016(6)$	$-0.0164(1)$	$-0.01741(9)$	$-0.01550(9)$	$-0.0123(1)$
6	$-0.0188(3)$	$-0.0189(2)$	$-0.0124(2)$	$-0.0069(1)$	$-0.00386(8)$
7	$-0.0227(3)$	$-0.0130(3)$	$-0.0053(1)$	$-0.00200(4)$	$-0.00070(1)$
8	$-0.0205(4)$	$-0.0072(1)$	$-0.00199(5)$		
9	$-0.0163(3)$	$-0.0036(1)$			
10	$-0.0115(5)$				
11	$-0.0083(2)$				
12	$-0.0056(3)$				
13	$-0.0043(5)$				

Table XVIII. R/B_2^{k-1}. The Underline Marks the Approximate Location of the Minimum Value

k	$D = 2$	$D = 3$	$D = 4$
3	$0.7824(2)$	$0.6248(2)$	$0.5063(2)$
4	$-0.01639(9)$	$-0.0298(1)$	$-0.0371(1)$
5	$0.00860(6)$	$0.01623(9)$	$0.0214(2)$
6	$-0.00526(8)$	$-0.0109(1)$	$-0.0150(2)$
7	$0.00335(6)$	$0.0078(2)$	$0.0124(2)$
8	$-0.00234(5)$	$-0.0064(1)$	$-0.0106(2)$
9	$0.00177(4)$	$0.0053(1)$	$0.0098(2)$
10	$-0.00125(3)$	$-0.00452(9)$	$-0.0091(2)$
11	$0.00095(2)$	$0.00392(8)$	$0.0089(2)$
12	$-0.00074(1)$	$-0.00333(7)$	$\underline{-0.0083(2)}$
13	$0.00055(1)$	$0.00313(8)$	$0.0086(2)$
14	$-0.00041(1)$	$-0.0027(1)$	$-0.0086(2)$
15	$0.00033(2)$	$\underline{0.0026(1)}$	$0.0087(3)$
16	$-0.00023(2)$		
17	$0.00021(3)$		

k	$D = 5$	$D = 6$	$D = 7$
3	$0.4139(2)$	$0.3409(2)$	$0.2822(2)$
4	$-0.03925(5)$	$-0.03815(8)$	$-0.0351(1)$
5	$0.0230(1)$	$0.02210(6)$	$0.02025(9)$
6	$-0.01689(9)$	$-0.0173(1)$	$-0.0153(2)$
7	$0.0142(3)$	$0.0144(2)$	$0.0135(2)$
8	$-0.0129(3)$	$-0.0141(3)$	$\underline{-0.0132(2)}$
9	$0.0126(2)$	$\underline{0.0138(3)}$	$0.0132(3)$
10	$\underline{-0.0126(3)}$	$-0.0150(3)$	$-0.0143(3)$
11	$0.0128(3)$	$0.0162(3)$	
12	$-0.0134(3)$	$-0.0172(3)$	
13	$0.0142(3)$	$0.0201(4)$	
14	$-0.0166(3)$	$-0.0238(5)$	
15	$0.0183(4)$	$0.0281(6)$	

Table XIX. R $(\diamondsuit)/B_2^{k-1} = R_{4,2}/B_2^{k-1}$. The Underline Marks the Approximate Location of the Minimum Value

k	D = 2	D = 3	D = 4	D = 5	D = 6
5	−0.01017(4)	−0.01654(7)	−0.01748(6)	−0.01551(4)	−0.01235(3)
6	0.00756(6)	0.01191(8)	0.01257(6)	0.01067(6)	0.00816(4)
7	−0.00607(8)	−0.01003(7)	−0.0106(1)	−0.00936(9)	−0.00737(7)
8	0.0051(1)	0.0088(2)	<u>0.0100(1)</u>	<u>0.00902(8)</u>	<u>0.00722(7)</u>
9	−0.00427(8)	−0.0083(1)	−0.0100(1)	−0.0095(2)	−0.00762(8)
10	0.00381(8)	0.0082(2)	0.0106(2)	0.0106(2)	
11	−0.00309(3)	−0.0075(1)	−0.0109(2)	−0.0116(2)	
12	0.00259(3)	0.00728(7)	0.0115(2)	0.0136(3)	
13	−0.00220(3)	−0.0071(3)	−0.0125(3)	−0.0156(3)	
14	0.00188(4)	0.0068(4)	0.0140(5)	0.0172(4)	
15	−0.00151(5)	−0.0060(5)	−0.0145(7)	−0.0227(7)	
16	0.00131(6)				
17	−0.00096(8)				

Table XX. R $(\diamondsuit)/B_2^{k-1} = R_{4,1}/B_2^{k-1}$. The Underline Marks the Approximate Location of the Minimum Value

k	D = 2	D = 3	D = 4	D = 5
5		−0.000242(2)	−0.000550(2)	−0.000765(4)
6		0.000435(3)	0.000984(7)	0.00137(1)
7	$-1.03(5) \times 10^{-8}$	−0.000342(5)	−0.00078(1)	−0.00112(1)
8	$5.0(2) \times 10^{-7}$	0.000294(6)	0.00076(1)	<u>0.00107(1)</u>
9	$-3.5(2) \times 10^{-6}$	−0.000290(6)	<u>−0.00073(1)</u>	−0.00108(2)
10	$8.6(4) \times 10^{-6}$	<u>0.000278(6)</u>	0.00074(1)	0.00121(2)
11	$-1.53(8) \times 10^{-5}$	−0.000281(6)	−0.00082(2)	−0.00135(3)
12	$1.83(9) \times 10^{-5}$	0.000273(8)	0.00085(2)	0.00154(3)
13	$-1.90(9) \times 10^{-5}$	−0.00029(1)	−0.00090(3)	−0.00178(4)
14	$2.1(1) \times 10^{-5}$	0.00028(2)	0.00104(4)	0.00205(5)
15	$-1.79(9) \times 10^{-5}$	−0.00026(2)	−0.00102(6)	−0.00244(9)
16	$1.6(1) \times 10^{-5}$			
17	$-1.3(1) \times 10^{-5}$			
18	$1.3(2) \times 10^{-5}$			

Table XXI. $R(\triangle)/B_2^{k-1} = R_{5,5}/B_2^{k-1}$

k	$D = 2$	$D = 3$	$D = 4$
6	0.00848(7)	0.01328(9)	0.01286(5)
7	−0.0063(1)	−0.0094(1)	−0.00947(9)
8	0.00469(9)	0.0078(1)	0.0081(1)
9	−0.00363(7)	−0.0065(1)	−0.00748(9)
10	0.00290(6)	0.0061(1)	0.0076(1)
11	−0.00230(8)	−0.0056(1)	−0.0072(1)
12	0.0020(1)	0.0051(1)	0.0075(2)
13	−0.0017(2)	−0.0045(2)	−0.0080(2)
14	0.0013(2)	0.0048(3)	0.0077(3)
15	−0.00097(24)	−0.0043(4)	−0.0087(5)

Table XXII. Pinwheel$/B_2^{k-1}$

k	$D = 2$	$D = 3$	$D = 4$
5	−0.0266(1)	−0.0315(1)	−0.02647(6)
6	0.00906(9)	0.01000(8)	0.00754(6)
7	−0.00194(4)	−0.00230(3)	−0.00178(3)
8	0.000187(4)	0.000302(6)	0.000261(5)
9	$-3.7(1) \times 10^{-6}$	−0.0000157(5)	−0.000022(1)
10	$2(1) \times 10^{-8}$	$5(1) \times 10^{-7}$	$8(4) \times 10^{-7}$

APPENDIX C. GRAPHS OF THE RATIO OF SELECTED DIAGRAMS TO HIGH ORDER

In this appendix we graph the ratios $B_k[4, 1]/B_k[0, 1]$, $B_k[5, 1]/B_k[0, 1]$, $R_{4, 2}/R$, $R_{4, 1}/R$, and $R_{5, 5}/R$ to orders up to $k = 17$.
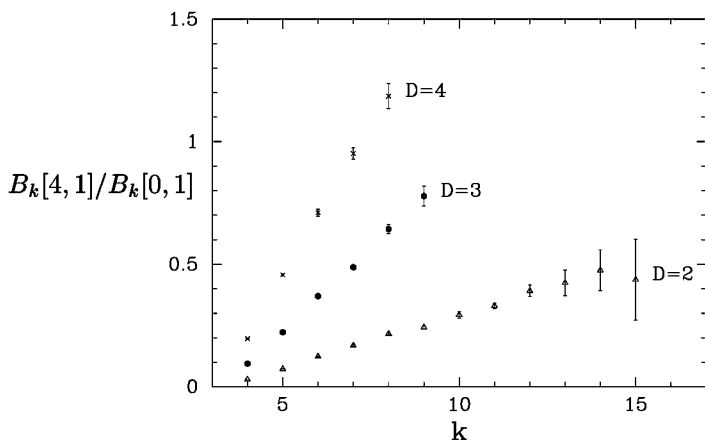
Fig. 1.   Absolute value of $\;\;/\varnothing = B_k[4, 1]/B_k[0, 1]$ in dimensions 2 (triangles), 3 (filled circles), and 4 (crosses).
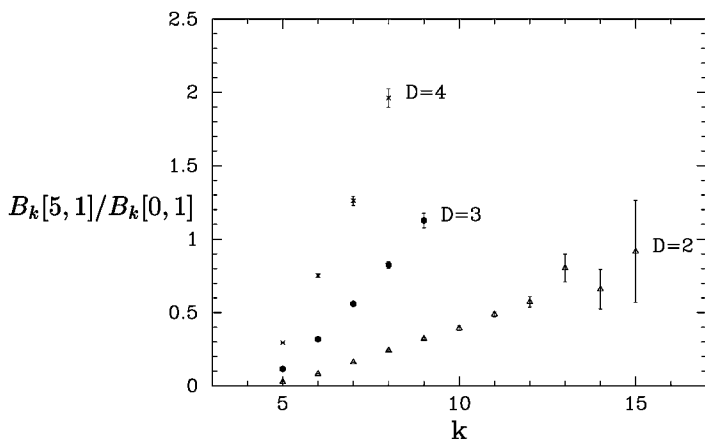
Fig. 2.   Absolute value of $\diagup/\varnothing = B_k[5, 1]/B_k[0, 1]$ in dimensions 2 (triangles), 3 (filled circles), and 4 (crosses).
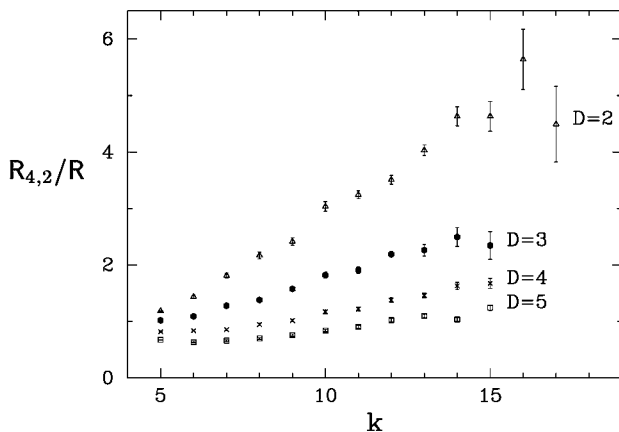
Fig. 3. Absolute value of $R(\langle\Diamond\rangle)/R = R_{4,2}/R$ in dimensions 2 (triangles), 3 (filled circles), 4 (crosses), and 5 (squares).
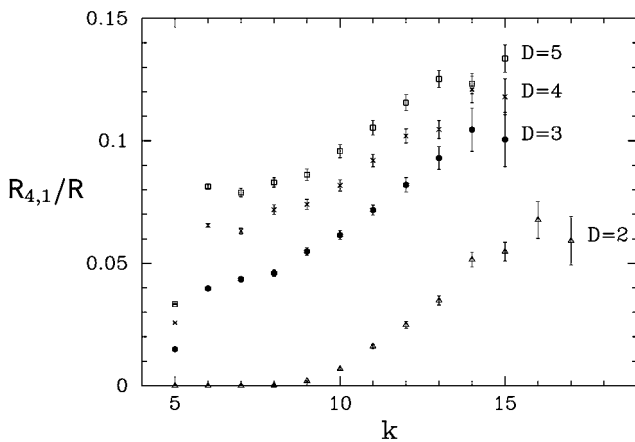
Fig. 4. Absolute value of $R(\langle\Diamond\rangle)/R = R_{4,1}/R$ in dimensions 2 (triangles), 3 (filled circles), 4 (crosses), and 5 (squares).
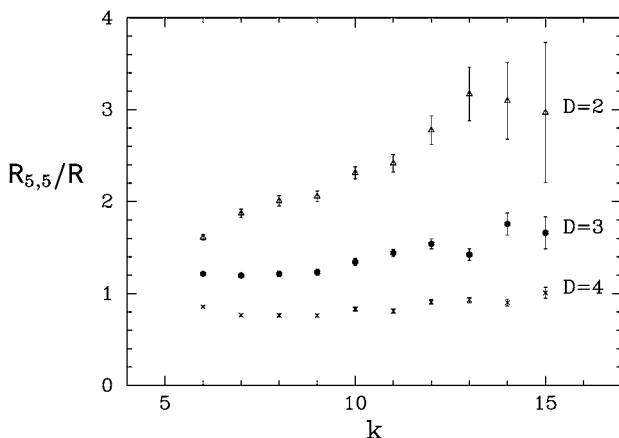
Fig. 5.   Absolute value of $R(\triangle)/R = R_{5,5}/R$ in dimensions 2 (triangles), 3 (filled circles), and 4 (crosses).

ACKNOWLEDGMENTS

REFERENCES

1. H. N. V. Temperley, Would a classical gas of non-attracting rigid spheres show a phase transition? *Proc. Phys. Soc. (London) B* **70**:536–537 (1957).
2. F. H. Ree and W. G. Hoover, On the signs of the hard sphere virial coefficients, *J. Chem. Phys.* **40**:2048–2049 (1964).
3. L. Tonks, The complete equation of state of one, two, and three-dimensional gases of hard elastic spheres, *Phys. Rev.* **50**:955–963 (1936).
4. L. Boltzmann, *Verslag. Gewone Vergadering Afd. Natuurk. Nederlandse Akad. Wtensch.* **7**:484 (1899).
5. J. S. Rowlinson, The virial expansion in two dimensions, *Mol. Phys.* **7**:593–594 (1964).
6. P. C. Hemmer, Virial coefficients for the hard-core gas in two dimensions, *J. Chem. Phys.* **42**:1116–1118 (1964).
7. J. J. van Laar, Berekening der tweede correctie op de grootheid *b* der toestandsvergelijking van der Waals, *Amsterdam Akad. Versl.* **7**:350–364 (1899).
8. B. R. A. Nijboer and L. van Hove, Radial distribution function of a gas of hard spheres and the superposition approximation, *Phys. Rev.* **85**:777–783 (1952).
9. F. H. Ree and W. G. Hoover, Fifth and sixth virial coefficients for hard spheres and hard discs, *J. Chem. Phys.* **40**:939–950 (1964).
10. K. W. Kratky, A new graph expansion of virial coefficients, *J. Stat. Phys.* **27**:533–551 (1982).

11. K. W. Kratky, Fifth to tenth virial coefficients of a hard-sphere fluid, *Physica A* **87**: 584–600 (1977).
12. K. W. Kratky, Overlap graph representation of b_6 and b_7, *J. Stat. Phys.* **29**:129–138 (1982).
13. E. J. Janse van Rensburg, Virial coefficients for hard discs and hard spheres, *J. Phys. A* **26**:4805–4818 (1993).
14. F. H. Ree and W. G. Hoover, Seventh virial coefficients for hard spheres and hard discs, *J. Chem. Phys.* **46**:4181–4196 (1967).
15. A. Y. Vlasov, X.-M. You, and A. J. Masters, Monte-Carlo integration for virial coefficients re-visited: Hard convex bodies, spheres with a square-well potential and mixtures of hard spheres, *Mol. Phys.* **100**:3313–3324 (2002).
16. M. Luban and A. Baram, Third and fourth virial coefficients of hard hyperspheres of arbitrary dimensionality, *J. Chem. Phys.* **76**:3233–3241 (1982).
17. N. Clisby and B. M. McCoy, Analytical calculation of B_4 for hard spheres in even dimensions, cond-mat/0303098.
18. M. Bishop, A. Masters, and J. H. R. Clarke, Equation of state of hard and Weeks–Chandler–Anderson hyperspheres in four and five dimensions, *J. Chem. Phys.* **110**:11449–11453 (1999).
19. E. Thiele, Equation of state for hard spheres, *J. Chem. Phys.* **39**:474–479 (1963).
20. M. S. Wertheim, Exact solution of the Percus–Yevick integral equation for hard spheres, *Phys. Rev. Lett.* **10**:321–323 (1963).
21. M. S. Wertheim, Analytic solution of the Percus–Yevick equation, *J. Math Phys.* **5**:643 (1964).
22. E. A. Guggenheim, Variations on van der Waals equation of state for high densities, *Mol. Phys.* **9**:199 (1965).
23. N. F. Carnahan and K. E. Starling, Equation of state for nonattracting rigid spheres, *J. Chem. Phys.* **51**:635–636 (1969).
24. W. G. Hoover and F. H. Ree, Melting transition and communal entropy for hard spheres, *J. Chem. Phys.* **49**:3609–3617 (1968).
25. R. Hoste and J. D. Dael, Equation of state for hard-sphere and hard-disk systems, *J. Chem. Soc. Faraday Trans. 2* **80**:477–488 (1984).
26. J. I. Goldman and J. A. White, Equation of state for the hard-sphere gas, *J. Chem. Phys.* **89**:6403 (1988).
27. E. J. Le Fevre, Equation of state for hard-sphere fluid, *Nature Phys.* **235**:20 (1972).
28. D. Ma and G. Ahmadi, An equation of state for dense rigid sphere gases, *J. Chem. Phys.* **84**:3449 (1986).
29. S. Jasty, M. Al-Naghy, and M. de Llano, Critical exponent for glassy packing of rigid spheres and disks, *Phys. Rev. A* **35**:1376–1381 (1987).
30. Y. Song, R. M. Stratt, and A. E. Mason, The equation of state of hard spheres and the approach to random closest packing, *J. Chem. Phys.* **88**:1126–1133 (1988).
31. X. Z. Wang, van der Waals–Tonks-type equations of state for hard-disk and hard-sphere fluids, *Phys. Rev. E* **66**:031203 (2002).
32. S. Torquato, Mean nearest-neighbor distance in random packings of hard D-dimensional spheres, *Phys. Rev. Lett.* **74**:2156–2159 (1995).
33. S. Torquato, Nearest-neighbor statistics for packings of hard spheres and disks, *Phys. Rev. E* **51**:3170–3182 (1995).
34. B. J. Alder and T. E. Wainwright, Phase transition for a hard sphere system, *J. Chem. Phys.* **27**:1208–1209 (1957).
35. B. J. Alder and T. E. Wainwright, Studies in molecular dynamics 2: Behavior of small numbers of elastic hard spheres, *J. Chem. Phys.* **33**:1439 (1960).

36. J. G. Kirkwood and E. Monroe, On the theory of fusion, *J. Chem. Phys.* **8**:845–846 (1940).
37. T. V. Ramakrishnan and M. Yussouff, 1st principles order-parameter theory of freezing, *Phys. Rev. B* **19**:2775–2794 (1979).
38. B. B. Laird, J. D. McCoy, and A. D. J. Haymet, Density functional theory of freezing: Analysis of crystal density, *J. Chem. Phys.* **87**:5449 (1987).
39. A. D. J. Haymet and D. W. Oxtoby, A molecular theory for freezing: Comparison of theories, and results for hard spheres, *J. Chem. Phys.* **84**:1769–1777 (1986).
40. W. G. Hoover and A. G. De Rocco, Sixth and seventh virial coefficients for the parallel hard-cube model, *J. Chem. Phys.* **36**:3141–3162 (1962).
41. R. J. Baxter, Three-colorings of the square lattice: A hard squares model, *J. Math. Phys.* **11**:3116–3124 (1970).
42. R. J. Baxter, Hard hexagons—Exact solution, *J. Phys. A* **13**:L61–70 (1980).
43. M. P. Richey and C. A. Tracy, Equation of state and isothermal compressibility for the hard hexagon model in the disordered regime, *J. Phys. A* **20**:L1121–L1126 (1987).
44. G. S. Joyce, On the hard-hexagon model and the theory of modular functions, *Phil. Trans. R. Soc. Lond. A* **325**:643–702 (1988).
45. J. E. Mayer and M. G. Mayer, *Statistical Mechanics* (Wiley, 1940).
46. F. H. Ree and W. G. Hoover, Reformulation of the virial series for classical fluids, *J. Chem. Phys.* **41**:1635–1645 (1964).
47. J. K. Percus and G. J. Yevick, Analysis of classical statistical mechanics by means of collective coordinates, *Phys. Rev.* **110**:1–13 (1958).
48. J. K. Percus, The pair distribution function in classical statistical mechanics, in *The Equilibrium Theory of Classical Fluids*, H. L. Frisch and J. L. Lebowitz, eds. (Benjamin, New York, 1964), pp. II-33–II-170.
49. F. Harary and E. M. Palmer, *Graphical Enumeration* (Academic Press, 1973).
50. B. D. McKay, Practical graph isomorphism, *Congr. Numer.* **30**:45–87 (1981).
51. L. M. Blumenthal, *Theory and Applications of Distance Geometry* (Clarendon Press, Oxford, 1953).
52. J. K. Percus, Dimensional reduction of integrals of orthogonal invariants, *Commun. Pure Appl. Math.* **40**:449–453 (1987).
53. J. G. Loeser, Z. Zhen, S. Kais, and D. R. Herschbach, Dimensional interpolation of hard sphere virial coefficients, *J. Phys. A.* **26**:4805–4818 (1993).
54. H. L. Frisch and J. K. Percus, High dimensionality as an organizing device for classical fluids, *Phys. Rev. E* **60**:2942–2948 (1999).
55. J. P. J. Michels and N. J. Trappeniers, Dynamical computer simulations on hard hyperspheres in four- and five-dimensional space, *Phys. Lett.* **104**:425–429 (1984).
56. R. Finken, M. Schmidt, and H. Löwen, Freezing transition of hard hyperspheres, *Phys. Rev. E* **65**:016108 (2001).
57. S. Katsura and Y. Abe, Irreducible cluster integrals of hard-sphere gases, *J. Chem. Phys.* **39**:2068–2079 (1963).
58. J. L. Lebowitz and O. Penrose, Convergence of virial expansion, *J. Math. Phys.* **5**:841 (1964).
59. A. Baram and M. Fixman, Rigorous bounds on the termination densities of hard disk and hard sphere fluids, *J. Chem. Phys.* **99**:5623–5624 (1993).
60. H. Reiss, H. L. Frisch, and J. L. Lebowitz, Statistical mechanics of rigid spheres, *J. Chem. Phys.* **31**:369–380 (1959).
61. J. D. Bernal and J. Mason, Coordination of randomly packed spheres, *Nature* **188**: 910–911 (1960).

62. J. D. Bernal, Bakerian lecture 1962—The structure of liquids, *Proc. Roy. Soc. London Ser. A* **280**:299–322 (1964).
63. G. D. Scott, Packing of equal spheres, *Nature* **188**:908–909 (1960).
64. J. L. Finney, Random packings and the structure of simple liquids I. The geometry of random close packing, *Proc. Roy. Soc. London Ser. A* **319**:479–493 (1970).